# Domain fluctuations in a ferroelectric low-strain BaTiO$_3$ thin film

Jianheng Li [1], Louie Zhong,[1] Rahul Jangid,[1] Meera,[1] Geoffery Rippy,[1] Kenneth Ainslie,[1] Chris Kohne,[1]
Arnoud S. Everhardt,[3] Beatriz Noheda,[3] Yugang Zhang,[2] Andrei Fluerasu,[2] Sylvia Matzen,[4] and Roopali Kukreja[1]

[1]*Department of Materials Science and Engineering, University of California, Davis, California 95616, USA*
[2]*National Synchrotron Light Source II (NSLS-II), Brookhaven National Laboratory, Upton, New York 11973, USA*
[3]*Zernike Institute for Advanced Materials, University of Groningen, 9747 AG Groningen, Netherlands*
[4]*Université Paris-Saclay, CNRS, Centre de Nanosciences et de Nanotechnologies, 91120 Palaiseau, France*

A ferroelectric BaTiO$_3$ thin film grown on a NdScO$_3$ substrate was studied using x-ray photon correlation spectroscopy (XPCS) to characterize thermal fluctuations near the $a/b$ to $a/c$ domain structure transformation present in this low-strain material, which is absent in the bulk. XPCS studies provide a direct comparison of the role of domain fluctuations in first- and second-order phase transformations. The $a/b$ to $a/c$ domain transformation is accompanied by a decrease in fluctuation timescales, and an increase in intensity and correlation length. Surprisingly, domain fluctuations are observed up to 25 °C above the transformation, concomitant with the growth of $a/c$ domains and coexistence of both domain types. After a small window of stability, as the Curie temperature is approached, $a/c$ domain fluctuations are observed, albeit slower, potentially due to the structural transformation associated with the ferroelectric to paraelectric transformation. The observed time evolution and reconfiguration of domain patterns highlight the role played by phase coexistence and elastic boundary conditions in altering fluctuation timescales in ferroelectric thin films.

## I. INTRODUCTION

The intriguing prospect of ferroelectric materials is that they possess spontaneous electric polarization that can be altered with applied electric fields [1–3]. Ferroelectric materials tend to form domains to minimize electrostatic and elastic strain energy [4–7]. A rich and flat energy landscape with a variety of single-, multi-, and metastable domain phases has been predicted for ferroelectric thin films as a function of misfit strain and temperature by first-principles calculation and Landau-Ginzburg-Devonshire model based theoretical studies [8–11]. These predictions have been experimentally confirmed for many ferroelectric systems, including BaTiO$_3$ (BTO) thin films, providing a unique approach for domain engineering [12–14]. The Landau-Ginzburg-Devonshire model assumes that fluctuations in the order parameter are significantly lower than the order parameter itself (polarization for ferroelectrics), but are critical while approaching the transition temperature. However, in systems with multiple nearly degenerate metastable states, dynamical fluctuations of domain patterns under specific strain and temperature conditions can not only control the stability and time evolution of the domain patterns, but can also play a significant role in the polarization switching and domain reconfiguration [1,15]. Dynamical fluctuations are also technologically relevant; for example, domain wall fluctuations in Ba$_{0.8}$Sr$_{0.2}$TiO$_3$ have recently been considered as a key reason for their superior gigahertz microwave tunability and ultralow dielectric losses [16], showing figure of merit values much greater than leading nonferroelectric piezoelectric systems, such as AlN [17–20]. Domain fluctuations are also closely related to data retention

in nonvolatile memories [21]. Thus, it is critical to develop a fundamental understanding of the mechanisms underlying domain fluctuations and their timescale evolution under different thermal and elastic conditions. However, the availability of techniques which can access both subnanometer length scales on fundamental timescales have been lacking. The sensitivity of atomic displacements in the picometer range to distinguish different polarization domains would allow access to dynamical fluctuations and to identify the mechanisms contributing to the energy landscape for domain reconfiguration, especially in the vicinity of a phase transition.

In this article, we utilized x-ray photon correlation spectroscopy (XPCS) to access both relevant timescales and length scales to study domain fluctuations and dynamics in a BaTiO$_3$ (BTO) thin film. BTO is a model system for lead-free ferroelectric materials [22–25]. It has recently been demonstrated that two different domain structures can be stabilized in BTO thin films grown on NdScO$_3$ (NSO) substrates with extremely low misfit strain ($\sim$0.05%) [12]. At room temperature a complex monoclinic domain structure forms, which can be simplified as a pseudo-orthorhombic $a/b$ phase, consisting of regions with spontaneous polarization alternating along the $a$ and $b$ crystallographic in-plane directions, with (110) domain walls separating the $a$ and $b$ domains. Near 55 °C, the domain structure is transformed to a complex pseudotetragonal $a/c$ domain structure [14], where $c$ denotes the out-of-plane direction, with the $a$ domains and $c$ domains separated by (101) domain walls. This transition is first order with a coexistence region of more than 10°. At 130 °C, the $a/c$ domain structure disappears as the system undergoes a ferroelectric to paraelectric phase transition.

We measured the temperature- and time-dependent intensity variation of the $a/c$ domain diffuse scattering, a superstructure due to the periodic domain ordering. The domain diffuse scattering peak was accessed close to the (001) Bragg peak to probe domain fluctuations in this low-strain BTO thin film across both transitions, the domain transformation from the in-plane $a/b$ to the out-of-plane $a/c$ domains near 55 °C (defined as the domain transformation temperature, $T_R$) and the ferroelectric to paraelectric transition near the Curie temperature, $T_C \sim 130$ °C. Our measurements show a strong temperature dependence of the timescales associated with domain fluctuations. Thermal fluctuations were observed to be most dramatic around 55 °C where the domain transformation occurs. The fluctuations associated with a concomitant increase in correlation length were observed up to 25 °C above $T_R$. As the temperature is raised slightly higher, the domains stabilize into a static pattern at around 90 °C. A further increase in temperature brings the system closer to the Curie temperature resulting in the observance of $a/c$ domain fluctuations. A compressed exponential shape of intermediate scattering function indicates the jamming behavior of both transitions as cooperative dynamics mediated by local strain relaxation.

## II. EXPERIMENTAL METHOD

A BTO (001) thin film (80 nm) was epitaxially grown on a NdScO$_3$ (NSO) substrate by pulsed laser deposition with a 6-nm SrRuO$_3$ (SRO) buffer layer. Dielectric permittivity and x-ray reciprocal space map (RSM) measurement confirming $T_R$ and $T_C$ are included in Supplemental Material [26] which includes Refs. [27–34]. Additional details of sample growth and x-ray characterization of the $a/b$ to $a/c$ domain transformation near $T_R$ can be found in Everhardt *et al.* [12]. XPCS experiments were conducted at the Coherent Hard X-ray Scattering (CHX) beamline at the National Synchrotron Light Source II (NSLS-II), Brookhaven National Laboratory. A coherent x-ray beam of 12.8 keV was focused on the thin film sample with a spot size of 3 $\mu$m through the collimation with a set of one-dimensional (1D) Be compound refractive lenses and focused with a set of crossed Si kinoform lenses. Figure 1(a) presents the scattering geometry utilized to access the $a/c$ domain diffuse scattering. The scattered beam was collected by a two-dimensional (2D) Eiger X 1M detector

(75 $\mu$m × 75 $\mu$m pixel size) positioned 1.5 m away from the sample. As the incident coherent x-ray beam undergoes scattering from the localized inhomogeneities (domains, defects, etc.) in the sample, it goes through constructive and destructive interference resulting in a "speckle" pattern on the detector as shown in Fig. 1(b). This speckle pattern was measured as a function of time for various temperatures from 35 °C to 125 °C. For each temperature step, the sample was stabilized for 30 min before beginning the XPCS scan to allow sufficient time to achieve thermal equilibrium. Details about the thermal stability can be found in Sec. 3 of the Supplemental Material [26].

## III. EXPERIMENTAL RESULTS

Figure 1(a) presents the $a/c$ domain diffuse scattering measured near the (001) Bragg reflection at $T = 40$ °C. The domain diffuse scattering arises due to the periodic arrangement of $a/c$ domains resulting in ordered domain walls. This results in periodic modulations of the diffuse scattering, which display increased intensity near the structural Bragg peak with the same periodicity as the domain walls [35,36]. This domain diffuse scattering is not observed at room temperature indicating that $a/c$ domains only form as the temperature approaches $T_R$ [12]. The speckles overlaying the domain diffuse scattering are the direct result of both the disorder present in the sample and the coherence of the x-ray beam. Figure 1(b) shows a line cut through the BTO domain diffuse scattering along the $Q_x$ axis, clearly showing the speckles. The Gaussian fit to the diffuse scattering pattern is identical to a peak profile under an incoherent beam, where localized information is averaged out by random phase of the incoherent diffracted beam [37].

The underlying domain fluctuations and their dynamics manifest themselves as a variation of this speckle pattern. Figure 2 presents these fluctuations as kymographs or "waterfall" plots for $T = 55$ °C, 90 °C, and 120 °C. The waterfall plots depict the evolution of intensity along a circular cut around the domain diffuse scattering as a function of time. Strong intensity variations were observed in the waterfall plots measured at 55 °C indicating fluctuations of the $a/c$ domains. As the temperature is increased to 90 °C, the speckle intensity stays relatively constant over a 2-h period, denoting exceptional stability of the $a/c$ domains. As the temperature
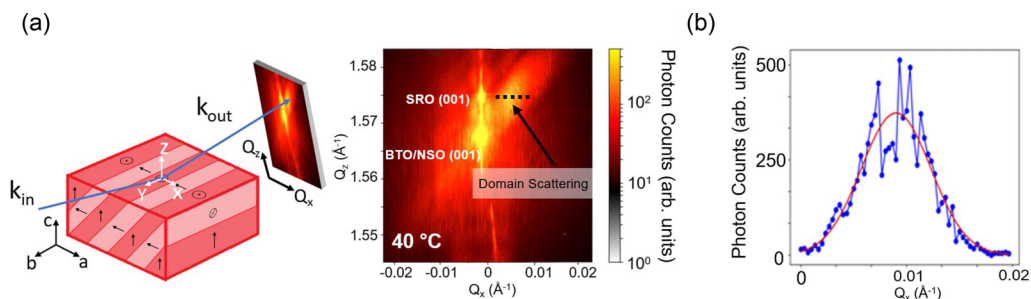


FIG. 1. (a) X-ray scattering geometry and the 2D detector image showing the (001) Bragg reflection from the BTO film, the substrate Bragg reflection and the $a/c$ domain diffuse scattering (note that $k_{in}$ is parallel to the $a/c$ domain walls). The sample temperature was 40 °C. (b) Speckle contrast obtained from the line cut through the domain diffuse scattering along the black dotted line shown in (a). A Gaussian function (red curve) was fitted to this line cut and used for calculating the domain correlation length.
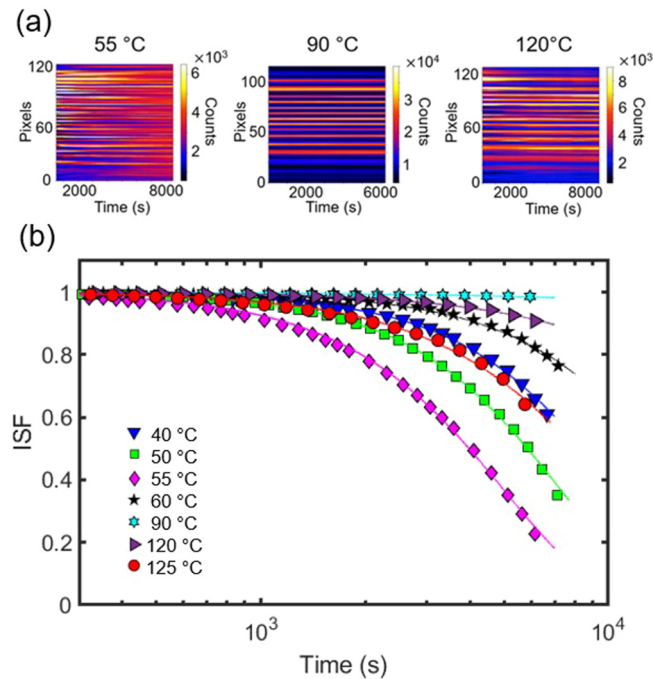
FIG. 2. (a) Kymographs or "waterfall plots" at 55 °C, 90 °C, and 120° C, demonstrating domain fluctuation and dynamics as a function of temperature. The waterfall plots are obtained by plotting the intensity as a function of time across a circular cut near the $a/c$ domain diffuse scattering. (b) Intermediate scattering function (ISF) and fits to the ISF calculated using Eqs. (1)–(2) for selected temperatures.

is raised to 120 °C (near $T_C$), intensity fluctuations are observed again, indicating faster dynamics as the ferroelectric to paraelectric transition is approached. The variation of speckle intensity in the waterfall plots for different temperatures directly demonstrates the strong temperature dependence of the domain dynamics.

Intensity-intensity autocorrelation functions, $g_2(Q, t)$, were calculated using Eq. (1) to quantify the overall intensity variation,

$$g_2(Q,t) = \frac{\langle I(Q,t)I(Q,t+\tau)\rangle}{\langle I(Q,t)\rangle^2}, \qquad (1)$$

where $I(Q,t)$ and $I(Q,t+\tau)$ are the intensity values of a given pixel separated in time by $\tau$ [38,39]. A spatial averaging over all pixels in the domain diffuse scattering is applied to evaluate this $g_2$ function. The calculated autocorrelation can be related to an intermediate scattering function (ISF), $F(Q,t)$, in the following manner,

$$g_2(Q,t) = 1 + A|F(Q,t)|^2 = 1 + A\left|e^{-\left(\frac{t}{\tau}\right)^\beta}\right|^2, \qquad (2)$$

where $A$ is the speckle contrast factor which is dependent on the experimental setup, background strength, and sample behavior; $\tau$ is the decay constant; and $\beta$ is the stretching exponent. Speckle contrast $A$ for all the measured temperatures in the experiment can be found in the Fig. S4 of the Supplemental Material [26]. A strong temperature dependence of the ISF is observed as shown in Fig. 2 for selected temperatures during a heating cycle. ISFs for all temperatures are included
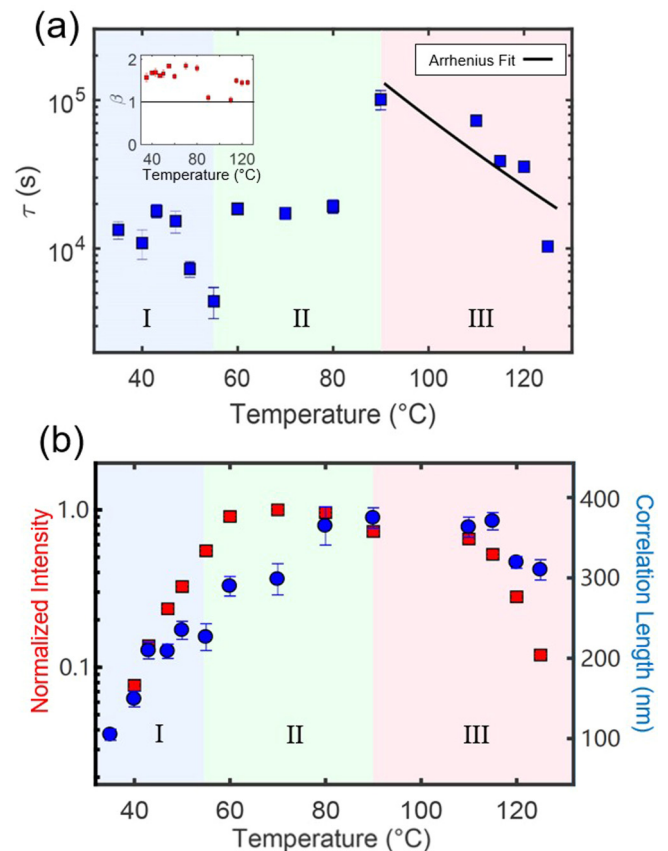


FIG. 3. (a) Characteristic domain fluctuation timescales ($\tau$) as a function of temperature obtained from the fits to the ISF shown in Fig. 2(b). The three regimes highlight the different behavior of timescales observed across the $a/b$ to $a/c$ domain transformation temperature, $T_R$, and Curie temperature, $T_C$. The solid line shows the Arrhenius fit for region III with an activation energy of $0.67 \pm 0.27$ eV. The inset shows the fitted stretched exponential value ($\beta$) as a function of temperature. A value of $\beta > 1$ is observed for all temperatures. (b) The normalized intensity of the $a/c$ diffuse scattering and the correlation length of the $a/c$ domains. The correlation length is calculated as described in the text.

in Fig. S5 of the Supplemental Material [26]. Here we note that no significant $Q$ dependence was observed and hence the $Q$ dependence was omitted from the $g_2$ and ISF calculations. The two-time correlation function was also plotted and no significant aging behavior was observed (see Supplemental Material [26]).

Figure 3(a) presents the obtained values of $\tau$ as a function of temperature. As the temperature is increased from 35 °C to 55 °C (regime I), a decrease of $\tau$ is observed, indicating higher fluctuations as $T_R$ is approached, where switching from the $a/b$ to $a/c$ domain structure occurs. With a further increase in temperature from 55 °C to 90 °C (regime II), $\tau$ jumps dramatically and stabilizes at 90 °C, where the ISF shows a flat line around 1, denoting a fully correlated system over the 2-h measurement period (see Fig. 2). Above 90 °C, as the temperature is raised to $T_C$ (regime III), a continuous decrease in $\tau$ is observed, indicating an increase in $a/c$ domain fluctuations as the Curie temperature is approached. This regime was fitted using the standard thermally activated

Arrhenius behavior, with an activation energy of 0.67 $\pm$ 0.27 eV. The inset of Fig. 3(a) shows the exponent, $\beta$, for the measured temperatures. We found the value of $\beta$ to be greater than 1, also shown by the compressed shape of the ISF for all the measured temperatures. A compressed exponential with $\beta > 1$ is indicative of jamming behavior in which local displacements can produce long-range inhomogeneities [40]. The jamming behavior is attributed to ultraslow ballistic motions as a result of relaxations driven by an internal stress field. A similar jamming behavior has been reported previously in ferroelectric $PbTiO_3/SrTiO_3$ superlattice thin films, materials exhibiting charge density waves, and magnetic and orbital ordering [41–43]. On the other hand, the exponential ($\beta = 1$) and the stretched exponential ($\beta < 1$) indicate diffusive and subdiffusive relaxation usually found in glass-forming liquids and colloidal suspensions, respectively [44–46].

Figure 3(b) shows the normalized intensity (red square symbols) of the $a/c$ domain diffuse scattering as a function of temperature for the three regimes. In regime I, it can be observed that the $a/c$ domain diffuse scattering appears at temperatures as low as 35 °C, and continues to grow as the temperature approaches $T_R$, indicating the formation and growth of $a/c$ domains. In regime II, where the temperature is raised to 90 °C, the intensity stays relatively constant. Finally, in regime III, as $T_C$ is approached, the intensity decreases concomitant with the ferroelectric to paraelectric phase transition and disappearance of $a/c$ domains. The observed Curie temperature of 130 °C is in agreement with the literature [12]. The dependence of the correlation length (blue circle symbols) on the temperature is also shown in Fig. 3(b). The correlation length, $\lambda$, was obtained from a fitted Gaussian profile as shown in Fig. 1(b), using $\lambda = 2\pi/\Delta Q$, where $\Delta Q$ is the full width at half maximum (FWHM) of the fitted Gaussian profile. An increase in $\lambda$ is observed from 35 °C to 80 °C indicating growth and a better ordering of $a/c$ domains as discussed below. At 90 °C, a FWHM value of $1.612 \times 10^{-3}$ Å$^{-1}$ is observed, resulting in a correlation length of 375 nm. As $T_C$ is approached, a decrease in correlation length is observed concomitant with a decrease in intensity as the ferroelectric to paraelectric transition occurs. Additionally, the striped domain periodicity, $d$, was calculated using $d = 2\pi/Q$, where $Q$ is the distance between domain diffuse scattering and Bragg peak along the $Q_x$ direction. A domain periodicity of 70 nm was calculated for the $a/c$ domains, and no temperature dependence was observed in the measured temperature range (Supplemental Material Fig. S7), in agreement with the literature [12,14,26].

## IV. DISCUSSION

The temperature-dependent domain dynamics across both transitions can be described by accounting for the variation of fluctuation timescale, domain diffuse intensity, and correlation length, across the three measured regimes. In regime I, during the early stages of $a/c$ domain formation near 35 °C, the amount of $a/c$ phase is low as shown by the integrated intensity with a relatively short correlation length (Fig. 3). As $T_R$ is approached, a transformation from the $a/b$ to the $a/c$ domain occurs, and hence the integrated intensity and correlation length increase dramatically, indicating the continual growth of $a/c$ domains. The correlation length increases

from 100 nm at 35 °C to 220 nm at 55 °C. On the other hand, it is noticeable that during the initial phase of regime I (from 35 °C to 45 °C), no obvious temperature dependence of domain fluctuation timescales is observed. This points to the fact that in the initial phase, the $a/c$ domains are growing (higher intensity and correlation length) in a predominantly $a/b$ matrix (also confirmed in Ref. [14]), and as the boundary conditions remain the same, the characteristic fluctuation timescales are also relatively constant. The fitted timescale of $a/c$ domain fluctuations is $\sim 1.3 \times 10^4$ s, which is comparable to the timescale in other ferroelectric systems far below the Curie temperature [41]. With a further increase in temperature (from 45 °C to 55 °C), a decrease in fluctuation timescales is observed as the transformation to the $a/c$ domains continues. Concomitant with faster fluctuations, the intensity and correlation length monotonically increase during the domain transformation resulting in a system which predominantly consists of $a/c$ domains.

In regime II, following the domain transformation, a slowdown of domain fluctuation is observed above 55 °C with significant jumps in $\tau$ from 55 °C to 60 °C and 80 °C to 90 °C. While the increase from 55 °C to 60 °C could be related to completion of domain transformation, the jump from 80 °C to 90 °C is surprising. Additionally, domain fluctuations are still observed up to 25 °C above $T_R$. During this temperature range, the correlation length continues to increase from 220 nm at 55 °C to 375 nm at 80 °C, reflecting an improved ordering of periodic $a/c$ domains at their equilibrium positions with the increase in temperature. As the intensity stays relatively unchanged during this period, this increase in correlation length is likely achieved by overcoming pinning due to defects or other pinning sites as temperature is raised. One of those pinning sites could be small fractions of remaining $a/b$ domains which have previously been observed up to at least 15 °C above $T_R$ [14]. Finally, near 90 °C, the system stabilizes and no fluctuations are observed due to no significant change in correlation lengths and complete disappearance of $a/b$ domains.

In regime III, as the Curie temperature is approached and more thermal energy is injected into the system, the fluctuation timescales decrease as the temperature increases. The diffuse scattering intensity and correlation length also decrease, indicating a reduction in the amount of $a/c$ domains. Remarkably, the decrease of fluctuation timescales, intensity, and correlation length signaling the nucleation and growth of the paraelectric phase begins 20 °C below the Curie temperature. From Fig. 3(b), it can be seen that the intensity drops much faster than the correlation length as the temperature is raised, i.e., intensity drops by 70% from 100 °C to 125 °C, while the correlation length has only decreased from 375 to 300 nm in the same temperature range. This observation shows that even as BTO is transforming to a cubic paraelectric phase, the remaining tetragonal ferroelectric domains show similar a periodicity and correlation length. Finally, near the Curie temperature, as the phase transition of the ferroelectric to paraelectric phase occurs, higher fluctuations with lower decay constant $\tau$ are observed. The estimated activation energy of 0.67 $\pm$ 0.27 eV in this regime is similar to the activation barrier for the migration of oxygen vacancies ($\sim$0.8 eV) observed for similar perovskites and which are considered as a source of domain wall pinning [47]. Alternatively, generation

and annihilation of topological defects has been reported as a potential mechanism for fluctuations of the ferroelectric domain pattern below the Curie temperature, which has an activation barrier of $0.35 \pm 0.21$ eV [41]. One or both of these processes could be occurring near the Curie temperature resulting in the observed fluctuation timescales.

It is interesting to note that the fluctuation timescales near the Curie temperature are longer than the timescales observed near the $a/b$ to $a/c$ domain transition, although the thermal energy injected into the system is higher, highlighting the different nature of the ferroelectric to paraelectric transition in comparison to ferroelectric to ferroelectric transition where domain rearrangement occurs. The significant variation of fluctuation timescales across the three regimes, including the observed fluctuations even 20 °C–25 °C above/below the transition temperature, depicts the complex energy landscape in this system with multiple states. It has been shown in PbZr$_{0.2}$Ti$_{0.8}$O$_3$ (PZT) thin films that the domains are relatively stable, and the thermal excitations alone are not enough to overcome the energy barriers between different metastable states [48–51]. Glassy behavior has been observed in PZT thin films due to competition between elasticity and pinning by a disorder potential. In contrast, precisely tuning the epitaxial strain in BTO lowers the energy difference between $a/b$ and $a/c$ domain states, resulting in a highly fluctuating system where domain dynamics are representative of jamming transitions. Only near 90 °C–100 °C (further away from $T_R$ or $T_C$), where no fluctuations are detected as the $a/c$ domains are stabilized, we observe a critical exponent closer to 1 which is typical of glassy systems. The domain stabilization observed in this temperature range could point towards similar behavior as PZT thin films.

## V. CONCLUSION

In conclusion, our XPCS measurements reveal the influence of phase coexistence on ferroelectric domain fluctuations and dynamics in low-strain BTO film. A compressed exponential with $\beta \sim 1.5$ indicates a jamming behavior for both the domain transformation transition at $T_R$, and the ferroelectric to paraelectric transition at $T_C$. Our studies also highlight the unique aspects of coherent x-ray techniques to access fundamental length scales and timescales critically required for studying the inherent role of domain fluctuations. The $a/b$ to $a/c$ domain transformation observed in this system and the faster timescales measured could provide a method to modify fluctuation timescales using domain engineering in ferroelectric systems as well as in other complex oxides. This is not only a key in understanding the fundamental role of domains in the thermal fluctuations at phase transformations, but can also provide a unique way to tune domain wall fluctuations to achieve, for example, technologically superior microwave tunability in ferroelectric based devices.

[1] J. F. Scott and C. A. Paz de Araujo, Ferroelectric memories, Science **246**, 1400 (1989).

[2] P. Muralt, Ferroelectric thin films for micro-sensors and actuators: A review, J. Micromech. Microeng. **10**, 136 (2000).

[3] D. L. Polla and L. F. Francis, Ferroelectric thin films in micro-electromechanical systems applications, MRS Bull. **21**, 59 (1996).

[4] A. Kopal, T. Bahnik, and J. Fousek, Domain formation in thin ferroelectric films: The role of depolarization energy, Ferroelectrics **202**, 267 (1997).

[5] L. Chen and A. L. Roytburd, 180° ferroelectric domains as elastic domains, Appl. Phys. Lett. **90**, 102903 (2007).

[6] S. Fernandez-Peña, C. Lichtensteiger, P. Zubko, C. Weymann, S. Gariglio, and J.-M. Triscone, Ferroelectric domains in epitaxial Pb$_x$Sr$_{1-x}$TiO$_3$ thin films investigated using x-ray diffraction and piezoresponse force microscopy, Appl. Phys. Lett. Mater. **4**, 086105 (2016).

[7] A. Torres-Pardo, A. Gloter, P. Zubko, N. Jecklin, C. Lichtensteiger, C. Collies, J.-M. Triscone, and O. Stéphan, Spectroscopic mapping of local structural distortions in ferroelectric PbTiO$_3$/SrTiO$_3$ superlattices at the unit-cell scale, Phys. Rev. B **84**, 220102(R) (2011).

[8] V. G. Koukhar, N. A. Pertsev, and R. Waser, Thermodynamic theory of epitaxial ferroelectric thin films with dense domain structures, Phys. Rev. B **64**, 214103 (2001).

[9] O. Diéguez, S. Tinte, A. Antons, C. Bungaro, J. B. Neaton, K. M. Rabe, and D. Vanderbilt, *Ab initio* study of the phase diagram of epitaxial BaTiO$_3$, Phys. Rev. B **69**, 212101 (2004).

[10] N. A. Pertsev and V. G. Koukhar, Polarization Instability in Polydomain Ferroelectric Epitaxial Thin Films and the Formation of Heterophase Structures, Phys. Rev. Lett. **84**, 3722 (2000).

[11] Z. Gui, S. Prosandeev, and L. Bellaiche, Properties of epitaxial (110) BaTiO$_3$ films from first principles, Phys. Rev. B **84**, 214112 (2011).

[12] A. S. Everhardt, S. Matzen, N. Domingo, G. Catalan, and B. Noheda, Ferroelectric domain structures in low-strain BaTiO$_3$, Adv. Electron. Mater. **2**, 1500214 (2016).

[13] A. S. Everhardt, T. Denneulin, A. Grünebohm, Y. Shao, P. Ondrejkovic, S. Zhou, N. Dominga, G. Catalan, J. Hlinka, J. Zuo, S. Matzen, and B. Noheda, Temperature-independent giant dielectric response in transitional BaTiO$_3$ thin films, Appl. Phys. Rev. **7**, 011402 (2020).

[14] A. S. Everhardt, S. Damerio, J. A. Zorn, S. Zhou, N. Domingo, G. Catalan, E. K. H. Salje, L. Chen, and B.

Noheda, Periodicity-Doubling Cascades: Direct Observation in Ferroelastic Materials, Phys. Rev. Lett. **123**, 087603 (2019).

[15] J. F. Scott, Electrocaloric materials, Annu. Rev. Mater. Res. **41**, 229 (2011).

[16] Z. Gu, S. Pandya, A. Samanta, S. Liu, G. Xiao, C. J. G. Meyers, A. R. Damodaran, H. Barak, A. Dasgupta, S. Saremi *et al.*, Resonant domain-wall-enhanced tunable microwave ferroelectrics, Nature **560**, 622 (2018).

[17] C. Zuo, J. V. Der Spiegel, and G. Piazza, 1.05-GHz CMOS oscillator based on lateral-field-excited piezoelectric AlN contour-mode MEMS resonators, IEEE Trans. Ultrason. Ferroelectr. Freq. Control **57**, 82 (2010).

[18] S. Gong, N. K. Kuo, and G. Piazza, GHz high-$Q$ lateral over-moded bulk acoustic-wave resonators using epitaxial SiC thin film, J. Microelectromech. Syst. **21**, 253 (2012).

[19] M. Rinaldi, C. Zuniga, C. Zuo, and G. Piazza, Super-high-frequency two-port AlN contour-mode resonators for RF applications, IEEE Trans. Ultrason. Ferroelectr. Freq. Control **57**, 38 (2010).

[20] M. Rinaldi, C. Zuniga, C. Zuo, and G. Piazza, 5–10 GHz AlN contour-mode nanoelectromechanical resonators, in *Proceedings of IEEE 22nd International Conference on Micro Electromechanical Systems, 2009 (MEMS)* (IEEE, Piscataway, NJ, 2009), p. 916.

[21] A. Sharma and A. Teverovsky, Preliminary Evaluation of Data Retention Characteristics for Ferroelectric Random Access Memories (FRAMs): NASA Goddard Space Flight Center Report (2001), pp. 1–4.

[22] E. J. H. Lee, F. M. Pontes, E. R. Leite, E. Longo, J. A. Varela, E. B. Araujo, and J. A. Eiras, Preparation and properties of ferroelectric $BaTiO_3$ thin films produced by the polymeric precursor method, J. Mater. Sci. Lett. **19**, 1457 (2000).

[23] P. C. Joshi and S. B. Desu, Structural, electrical, and optical studies on rapid thermally processed ferroelectric $BaTiO_3$ thin films prepared by metallo-organic solution deposition technique, Thin Solid Films **300**, 289 (1997).

[24] M. N. Kamalasanan, N. Deepak Kumar, and S. Chandra, Dielectric and ferroelectric properties of $BaTiO_3$ thin films grown by the sol-gel process, J. Appl. Phys. **74**, 5679 (1993).

[25] Y. Yoneda, T. Okabe, K. Sakaue, and H. Terauchi, Structural characterization of $BaTiO_3$ thin films grown by molecular beam epitaxy, J. Appl. Phys. **83**, 2458 (1998).

[26] See Supplemental Material at http://link.aps.org/supplemental/10.1103/PhysRevMaterials.4.114409 for details on preliminary characterization of domain structure, beam coherence, beamline stability, ISF plot for all temperatures, two-time $g_2$, and domain periodicity, which includes Refs. [27–34].

[27] K. G. Wilson, Renormalization group and critical phenomena. II. Phase-space cell analysis of critical behavior, Phys. Rev. B **4**, 3184 (1971).

[28] M. Stengel, D. Vanderbilt, and N. A. Spaldin, Enhancement of ferroelectricity at metal-oxide interfaces, Nat. Mater. **8**, 392 (2009).

[29] B. -K. Lai, I. A. Kornev, L. Bellaiche, and G. J. Salamo, Phase diagrams of epitaxial $BaTiO_3$ ultrathin films from first principles, Appl. Phys. Lett. **86**, 132904 (2005).

[30] S. Tinte and M.G. Stachiotti, Surface effects and ferroelectric phase transitions in $BaTiO_3$ ultrathin films, Phys. Rev. B **64**, 235403 (2001).

[31] T. Sluka, A. K. Tagantsev, D. Damjanovic, M. Gureev, and N. Setter, Enhanced electromechanical response of ferroelectrics due to charged domain walls, Nat. Commun. **3**, 748 (2012).

[32] X. M. Chen, V. Thampy, C. Mazzoli, A. M. Barbour, H. Miao, G. D. Gu, Y. Cao, J. M. Tranquada, M. P. M. Dean, and S. B. Wilkins, Remarkable Stability of Charge Density Wave Order in $La_{1.875}Ba_{0.125}CuO_4$, Phys. Rev. Lett. **117**, 167001 (2016).

[33] J. Verwohlt, M. Reiser, L. Randolph, A. Matic, L. A. Medina, A. Madsen, M. Sprung, A. Zozulya, and C. Gutt, Low Dose X-Ray Speckle Visibility Spectroscopy Reveals Nanoscale Dynamics in Radiation Sensitive Ionic Liquids, Phys. Rev. Lett. **120**, 168001 (2018).

[34] O. Czakkel and A. Madsen, Evolution of dynamics and structure during formation of a cross-linked polymer gel, Europhys. Lett. **95**, 28001 (2011).

[35] P. Zubko, N. Stucki, C. Lichtensteiger, and J.-M. Triscone, X-Ray Diffraction Studies of 180° Ferroelectric Domains in $PbTiO_3/SrTiO_3$ Superlattices under an Applied Electric Field, Phys. Rev. Lett. **104**, 187601 (2010).

[36] P. Zubko, N. Jecklin, N. Stucki, C. Lichtensteiger, G. Rispens, and J.-M. Triscone, Ferroelectric domains in $PbTiO_3/SrTiO_3$ superlattices, Ferroelectrics **433**, 127 (2012).

[37] B. Lengeler, Coherence in x-ray physics, Naturwissenschaften **88**, 249 (2001).

[38] A. Nogales and A. Fluerasu, X ray photon correlation spectroscopy for the study of polymer dynamics, Eur. Polym. J. **81**, 494 (2016).

[39] O. G. Shpyrko, X-ray photon correlation spectroscopy, J. Synchrotron Radiat. **21**, 1057 (2014).

[40] L. Cipelletti, L. Ramos, S. Manley, E. Pitard, D. A. Weitz, E. E. Pashkovski, and M. Johansson, Universal non-diffusive slow dynamics in aging soft matter, Faraday Disc. **123**, 237 (2003).

[41] Q. Zhang, E. M. Dufresne, P. Chen, J. Park, M. P. Cosgriff, M. Yusuf, Y. Dong, D. D. Fong, H. Zhou, and Z. Cai, Thermal Fluctuations of Ferroelectric Nanodomains in a Ferroelectric-Dielectric $PbTiO_3/SrTiO_3$ Superlattice, Phys. Rev. Lett. **118**, 097601 (2017).

[42] O. G. Shpyrko, E. D. Isaacs, J. M. Logan, Y. Feng, G. Aeppli, R. Jaramillo, H. C. Kim, T. F. Rosenbaum, P. Zschack, and M. Sprung, Direct measurement of antiferromagnetic domain fluctuations, Nature **447**, 68 (2007).

[43] R. Kukreja, N. Hua, J. Ruby, A. Barbour, W. Hu, C. Mazzoli, S. Wilkins, E. E. Fullerton, and O. G. Shpyrko, Orbital Domain Dynamics in Magnetite below the Verwey Transition, Phys. Rev. Lett. **121**, 177601 (2018).

[44] B. Ruta, G. Baldi, Y. Chushkin, B. Rufflé, L. Cristofolini, A. Fontana, M. Zanatta, and F. Nazzani, Revealing the fast atomic motion of network glasses, Nat. Commun. **5**, 3939 (2014).

[45] R. Angelini, L. Zulian, A. Fluerasu, A. Madsen, G. Ruocco, and B. Ruzicka, Dichotomic aging behaviour in a colloidal glass, Soft Matter **9**, 10955 (2013).

[46] A. Fluerasu, A. Moussaïd, A. Madsen, and A. Schofield, Slow dynamics and aging in colloidal gels studied by x-ray photon correlation spectroscopy, Phys. Rev. E **76**, 010401 (2007).

[47] L. He and D. Vanderbilt, First-principles study of oxygen-vacancy pinning of domain walls in $PbTiO_3$, Phys. Rev. B **68**, 134103 (2003).

[48] P. Paruch, T. Giamarchi, T. Tybell, and J.-M. Triscone, Nanoscale studies of domain wall motion in epitaxial ferroelectric thin films, J. Appl. Phys. **100**, 051608 (2006).

[49] P. Paruch, A. B. Kolton, X. Hong, C. H. Ahn, and T. Giamarchi, Thermal quench effects on ferroelectric domain walls, Phys. Rev. B **85**, 214115 (2012).

[50] P. Paruch, T. Giamarchi, and J.-M. Triscone, Domain Wall Roughness in Epitaxial Ferroelectric $PbZr_{0.2}Ti_{0.8}O_3$ Thin Films, Phys. Rev. Lett. **94**, 197601 (2005).

[51] T. Tybell, P. Paruch, T. Giamarchi, and J.-M. Triscone, Domain Wall Creep in Epitaxial Ferroelectric $Pb(Zr_{0.2}Ti_{0.8})O_3$ Thin Films, Phys. Rev. Lett. **89**, 097601 (2002).